JOURNAL OF THERMOPHYSICS AND HEAT TRANSFER
Vol. 22, No. 3, July–September 2008

Numerical Investigation of a Radial Microchannel Heat Exchanger with Varying Cross-Sectional Channels

R. Muwanga, I. Hassan,* and M. Ghorab
Concordia University, Montreal, Quebec H3G 1M8, Canada

DOI: 10.2514/1.33189

This paper investigates the heat transfer performance of a radial microchannel heat exchanger with varying cross-sectional-area channels. The thermal performance of axially varying cross-sectional-area channels is compared with uniform cross-sectional-area channels. The first model is a one-dimensional thermal-resistance based model, and the second model is a three-dimensional conjugate computational fluid dynamics analysis using FLUENT software. The heat sink has a footprint area of 3.5 cm^2 and the fluid flows radially inward. The inlet aspect ratio is varied from 0.4 to 1.0, and the outlet aspect ratio is fixed at 0.5. Inclusion of axial conduction effects are found to be imperative for accurate modeling of a radial configuration using the one-dimensional thermal-resistance model. The analysis shows that when constrained by a fixed channel-outlet area, increasing the channel-inlet area will improve the thermal performance. At low pumping powers, the present scheme is found to have thermal performance that is equivalent to or better than the performances with other experimentally and numerically investigated microchannel heat sink designs.

Nomenclature

$A_{3/4}$	=	three- or four-wall-heated area
Cp	=	specific heat capacity, kJ/(kg · K)
D_h	=	hydraulic diameter, m
f	=	friction factor
H	=	height, m
q''	=	heat flux, W/m^2
k	=	thermal conductivity, W/(m · K)
L	=	length, m
$\dot{m}$	=	mass flow rate, kg/s
N_{chn}	=	number of channels
Nu	=	Nusselt number
P	=	pressure, Pa
Pr	=	Prandtl number
R	=	thermal resistance, K/W
Re	=	Reynolds number based on hydraulic diameter
r	=	radial coordinate, m
r^+	=	$(r_o - r)/(r_o - r_i)$
T	=	temperature, K
V	=	velocity, m/s
W	=	width, m
z	=	streamwise coordinate, m
z^+	=	z/L_{chn}
z^*	=	$z/RePrD_h$
α	=	channel aspect ratio (width/height)
β_1	=	unit cell angle
β_2	=	channel angle
θ	=	nondimensional temperature
μ	=	dynamic viscosity, N · s/m^2
ν	=	kinematic viscosity, m^2/s
ρ	=	density, kg/m^3

Subscripts

b	=	fluid bulk parameter
chn	=	channel parameter
i	=	inner radius parameter
in	=	inlet parameter
j	=	counter
o	=	outer radius parameter
out	=	outlet parameter
w	=	wall parameter

Introduction

ADVANCES in microelectromechanical systems (MEMS)-based manufacturing has seen the creation and the development of a number of miniaturized technologies, from DNA analysis [1] to power generation [2]. Related to thermal management via microfabrication technologies, the microchannel heat sink is a prime contender for high heat flux management and is currently being investigated by a number of researchers. Tuckerman and Pease [3] pioneered this device in the early 1980s using a wet-etched 50-μm-wide and 300-μm-deep silicon-microchannel heat sink. Under single-phase flow conditions with deionized water, they were able to demonstrate heat dissipation up to 790 W on a 1-cm^2 chip.

Current investigations are considering alternatives to the standard straight parallel-channel microheat sink with the aim of decreasing the pressure drop and enhancing the heat transfer. Among these, single-phase flow studies have considered pin fins [4,5], fractal and constructal schemes [6–9], and cross-linked channels [10–12]. Furthermore, the fractal and constructal schemes are the only schemes to use radial flow. One of the motivations of these two schemes is the possibility of reducing the pressure drop. Alharbi et al. [8] and Pence [9] considered a radially-outward-flowing fractal network. Three-dimensional numerical simulations of this configuration have shown improved surface temperature uniformity. This configuration also had a pressure increase, however, the design was not optimized.

Bau [13] proposed the use of channels with slowly varying cross sections for improving the thermal performance of micro heat exchangers. The author showed that through optimizing the wall contour with streamwise distance, the maximum wall temperature, or the maximum wall gradient, could be minimized in comparison with straight parallel channels. To determine the optimum channel profiles, first- or second-order polynomials were used. An objective function was determined, relating wall temperature to cross-sectional area, by considering calorimetric and cross-sectional resistances. Optimum configurations were determined based on a fixed pressure drop, channel depth, viscosity, and channel length. This approach assumed the flow to be locally fully developed and incompressible. It neglected the variation in fluid properties due to temperature, the

Received 2 July 2007; revision received 27 October 2007; accepted for publication 28 October 2007.

*Department of Mechanical and Industrial Engineering; Associate Professor; ibrahimH@alcor.concordia.ca (Corresponding Author).

pressure drop due to acceleration, and axial conduction. The local Nusselt number and Poisuelle number were determined from the fully developed analytical solutions as a function of local channel aspect ratios.

There have been a number of investigations considering flow without heat transfer in channels of slowly varying cross sections. One of the first studies was by Mantion [14], who considered incompressible steady flow in a circular tube with a Reynolds number on the order of unity. Through the use of an asymptotic series solution, the author showed that the local flow conditions could be approximated as Poisuelle flow with first-order error. Recently, Lauga et al. [15] analytically investigated flows in channels with fixed wall heights and varying widths or curvature. They demonstrated that Stokes flow in rectangular ducts with slowly varying width is inevitably three-dimensional.

Studies considering flow with heat transfer in slowly varying ducts, however, are limited, partially due to their limited applicability to heat exchangers. Brod [16] considered flow in a circular tube and a two-dimensional plane channel of a slowly varying cross section and directed at the process industries using melts. Assuming a similarity solution, whereby the velocity at each cross section was fully developed, the author obtained expressions for the fluid bulk temperature and heat transfer distribution. The study showed the nondimensional fluid bulk temperature and the local Nusselt number to be invariant on the tube's contour function. Additionally, the heat transfer was only dependent on the Fourier number in the case of a circular tube and on the effective Fourier number in the case of parallel plates. Tapered channels are typical in the internal cooling schemes of gas turbine airfoils; however, researchers have only recently been investigating the influence of the varying cross section on heat transfer [17]. MEMS-based fabrication can readily produce rectangular channels with variable widths. In the work of Li et al. [1], a polymerase chain reaction microchip with serpentine microchannels of varying width was designed and fabricated for control of the velocity at different areas of the chip. Velocity control optimized the sample exposure times at the different temperature phases while minimizing the transition time during temperature-phase transition.

A potential benefit of a radially flowing heat exchanger is the ability to easily incorporate varying cross-sectional-area channels into the geometry: for example, linearly converging channels for radially inward flow or linearly diverging channels for radially outward flow. Few works are available on the convective heat transfer characteristics of channels with slowly varying cross sections that were highlighted in this review. Further, to the authors' knowledge, no works have performed a three-dimensional numerical investigation of channels with slowly varying cross sections for micro-heat-exchanger applications. In the first part of this paper, a thermal-resistance model is adapted for use in radially-inward-flow channels with varying cross section. The analysis evaluates the characteristics and benefits of flow in channels of varying cross sections. In the second part of the paper, a similar investigation is performed, except with a three-dimensional conjugate heat transfer model.

The analysis is based on a heat exchanger design proposed by Muwanga [18]. The specifications for the proposed design were to maintain a maximum temperature of 85°C given a heat flux of 25 W/cm^2 with a 3.5-cm^2 footprint area and a pressure availability of 34.47 kPa (5 psi). Uniform channels were considered in the design and the heat sink was sized for these specifications. The channels were fabricated in a silicon substrate via deep reactive ion etching with 300-μm-deep channels. Additional constraints introduced for structural integrity and handling included a central plenum of 1 mm and a minimum wall fin thickness of 50 μm. A schematic of this proposed design is shown in Fig. 1. Fabrication trials were performed, but no experimental measurements were obtained.

Thermal Resistance Analysis

Mathematical Model

The present model is an adaptation of the model by Bau [13], which only considered a three-wall-heated boundary condition under fully developed flow conditions. This model was a one-dimensional thermal-resistance network model that assumed steady-state, laminar, and incompressible flow within a heated parallel-channel system. The present adaptations are four-wall heating, four-wall heating with thermally developing flow, and radially configured channels. Thermally developing flow is more realistic for microsystems because, due to the large pressure drop, short channels are usually encountered. The fluid properties are taken as constant viscous dissipation and axial conduction is neglected, as is heat transfer due to natural convection and radiation.

The modeled region consists of a unit cell, as depicted in Fig. 2. This cell consists of a single channel with a fixed height H_{chn} and length L_{chn}, which spans the outer r_o to inner r_i radius. The wall-thickness resistance is neglected, assuming that the material has a high thermal conductivity. The channel width is defined as some continuous function of the axial location $W_{\text{chn}}(r) = r\beta_2$, whereas the channel height is constant. The channel aspect ratio, defined as the width-to-height ratio, is consequently a function of the radial location $\alpha = W_{\text{chn}}(r)/H_{\text{chn}}$.

The total thermal resistance is a combination of the convective R_{conv} and calorimetric R_{cal} thermal resistances. Considering

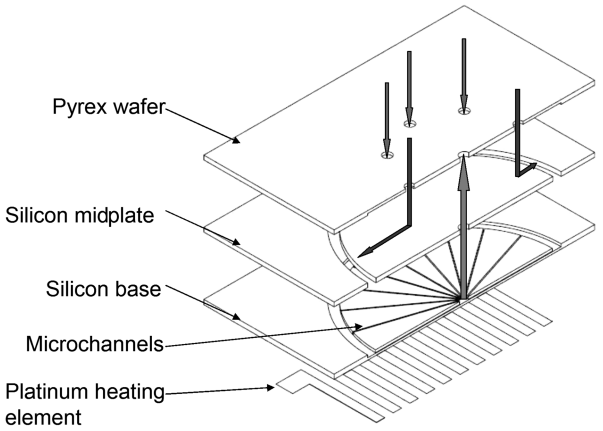

Fig. 1 Radial silicon-microchannel heat sink from Muwanga [18]; depiction of radially inward flow.

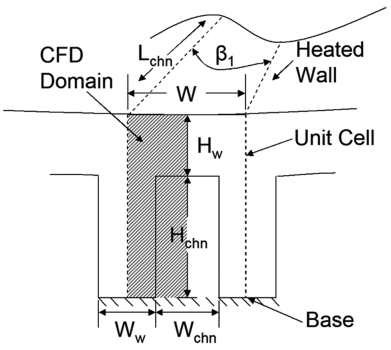

a) Cross-sectional view

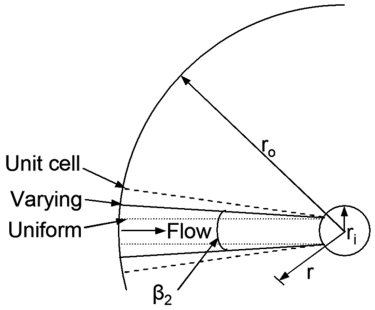

b) Top view

Fig. 2 Modeling domain depiction.

convective transport within a single channel with a heat flux applied on the top outer wall results in

$$\left[\frac{q''\pi(r_o^2 - r_i^2)}{N_{\text{chn}}}\right] \Big/ A_{3/4} = h(r)(T_w(r) - T_b(r)) \tag{1}$$

The inner-wall heated area is denoted by $A_{3/4}$ for three- or four-wall-heated scenarios. The convective thermal resistance is then be derived as

$$R_{\text{conv}} = \theta_w(r) - \theta_b(r) = \frac{2\alpha\pi(r_o^2 - r_i^2)}{Nu(r)\cdot(1+\alpha)[L_{\text{chn}}H_{\text{chn}}([(\alpha_o + \alpha_i)/2] + 2)]N_{\text{chn}}} \tag{2}$$

for a three-wall-heated channel and

$$R_{\text{conv}} = \theta_w(r) - \theta_b(r) = \frac{2\alpha\pi(r_o^2 - r_i^2)}{Nu(r)\cdot(1+\alpha)[2L_{\text{chn}}H_{\text{chn}}([(\alpha_o + \alpha_i)/2] + 1)]N_{\text{chn}}} \tag{3}$$

for a four-wall-heated channel, and θ is the nondimensional temperature defined as

$$\theta(r) = \frac{T(r) - T_{b,o}}{q''H_{\text{chn}}/k} \tag{4}$$

Numerically derived solutions of the Nusselt number under fully developed flow for cases of three- and four-wall-heated conditions, may be obtained from Shah and London [19] as a function of aspect ratio. Similar to Bau [13], the solutions for constant-periphery wall temperature are taken. For thermally developing flow, Lee and Garimella [20] recently provided a correlation based on numerical solutions for four-wall-heated conditions with constant heat flux (as opposed to constant-periphery wall temperature). This correlation was selected because data are not readily available for a constant-periphery wall temperature for a variety of aspect-ratio channels and under thermally or simultaneously developing flow conditions.

For the calorimetric thermal resistance, an energy balance within the channel gives

$$\frac{q''\pi(r_o^2 - r^2)}{N_{\text{chn}}} = \dot{m}Cp(T_b(r) - T_b(r_o)) \tag{5}$$

Following the considerations by Bau [13], we have the calorimetric thermal resistance defined as

$$R_{\text{cal}} = \theta_b(r) = \frac{\pi\{r_o^2 - (r_o - r^+(r_o - r_i))^2\}}{N_{\text{chn}}}\left(\frac{k_b}{Cp}\right)\left(\frac{1}{\dot{m}^*\cdot\dot{m}_0 H_{\text{chn}}}\right) \tag{6}$$

where

$$r^+ = \frac{r_o - r}{r_o - r_i} \tag{7}$$

and

$$\dot{m}^* = 1 \Big/ \int_0^1 \frac{1}{8} Po(\alpha)\frac{(1+\alpha)^2}{\alpha^3}\,\mathrm{d}r^+ \tag{8}$$

The parameter $\dot{m}_o$ is the characteristic mass flow rate parameter given by

$$\dot{m}_0 = \frac{H_{\text{chn}}^4 \Delta P}{\nu L_{\text{chn}}} \tag{9}$$

To obtain the preceding definition of calorimetric thermal resistance, Bau [13] assumed the flow to be locally fully developed within the channel and the pressure drop due to acceleration to be negligible. The Poiseuille number $Po(\alpha)$ was obtained from Shah and London [18] and is given by

$$Po(\alpha) = fRe = 96[1 - 1.3553\alpha + 1.94673\alpha^2 - 1.7012\alpha^3 + 0.9564\alpha^4 - 0.2537\alpha^5] \tag{10}$$

This is a correlation for numerical solutions of fully developed flow within a channel of aspect ratio α. The total thermal resistance is then obtained from summation of the calorimetric and convective resistances. This is, equivalently, the wall temperature:

$$R_{\text{tot}} = \theta_w(r) = R_{\text{conv}} + R_{\text{cal}} \tag{11}$$

Problem Analysis

The performance criterion evaluated is the channel configuration that produces the smallest peak wall temperature and is defined as

$$\min[\max\{\theta_w(r)\}] \tag{12}$$

The aspect ratio may be defined as an Nth-order polynomial:

$$\alpha(r) = \sum_{j=0}^{N} \alpha_i r^j \tag{13}$$

For the present study, linear polynomials are considered. The minimization of Eq. (12) was performed using a golden-section search and parabolic interpolation-minimization routine available using the MATLAB `fminbnd` and `fminsearch` functions. The `fminbnd` function is a one-parameter minimization routine and was used to optimize the uniform channel configurations. The `fminsearch` function is a multiparameter minimization routine and was used for the varying cross-sectional-area channel searches. This function may produce local minima and hence was found to sometimes be start-point-dependent. For this reason, the channel configurations using this multiparameter function are not identified as optimum, but improved.

General inputs for the analysis include a channel depth of 300 μm and outer and inner radii of 11.05 and 0.5 mm, respectively. These are based on consideration of a heat exchanger with a 3.5-cm^2 footprint area. The working fluid is water, with properties set at 298 K. Restrictions are placed on the channel width and the fin width at the exit to be a minimum of 50 μm.

One-Dimensional Resistance Model Results

The resulting channel configurations using the developed one-dimensional thermal-resistance analysis for radially-inward-flowing channels and for a variety of boundary conditions are presented in Figs. 3–5. For the present conditions, at a heat flux of 25 W/cm^2, a difference in θ_w of 0.01 translates into a temperature difference of approximately 1.2 K. In all cases, a lower peak temperature is obtained by using a converging channel. Looking at the uniform cross-sectional-area channels, a consistent trend is observed. This trend shows a decreasing channel width with increasing pressure availability. The increased pressure availability allows for smaller channel diameters, which in turn improves the thermal performance. This is due to both higher heat transfer coefficients and increased convective surface area, due to more channels. For the channels with varying cross-sectional areas, however, such a trend is not readily observed. Comparing the channels with varying cross-sectional areas with uniform channels, in all cases, the varying cross-sectional-area channels have a wider inlet and a narrower exit for a given pressure drop. This is possible because the wider inlet provides a lower frictional resistance, and this added benefit may then be used at the narrower exit. The resulting wall profiles for the fully developed cases approach each other, both for uniform and varying cross-sectional configurations, as the available pressure increases. The resulting nondimensional temperatures are also similar, however, the magnitudes may vary substantially when considering the dimensional values.

Observing the wall-temperature profiles, in all cases, a nonlinear rise in wall temperature is obtained. For four-wall-heated fully developed (Figs. 4a and 4b) vs thermally developing flow (Figs. 5a

and 5b), a more realistic temperature profile is obtained. For this profile, the initial wall to fluid temperature difference approaches zero and rises rapidly, due to the developing thermal boundary layer. Comparing Figs. 4a and 5a for the uniform channels, the influence of fully developed vs a thermally developing profile influences the entrance characteristics. The exit temperatures, however, are similar and the peak occurs at the exit. Therefore, in terms of minimizing the peak temperature, if considering uniform channels, fully developed and thermally developing flows will provide a similar conclusion. However, this is substantially different when considering a channel with linearly varying cross section in a radial configuration. Although the exit temperatures are similar in magnitude, the peak does not necessarily occur at the exit. Subsequently, the improved configuration can be significantly different, depending on whether fully developed or thermally developing flow is used.

Three-Dimensional Conjugate Analysis

The results presented in the previous section are limited by the incorporated assumptions. Particular assumptions that may have significance for actual microchannel systems are the flow development (thermally and hydrodynamically), negligible axial conduction, and constant fluid properties. An investigation was carried out on a radially-inward-flowing micro heat exchanger using a three-dimensional conjugate heat transfer model.

Formulation and Solution Methodology

The computational domain consists of one-half of a unit cell (shaded region), depicted in Fig. 2a, spanning the full radius. The heat exchanger has a footprint area of 3.5 cm^2 with an outer radius r_o of 11.05 mm and an inner radius r_i of 0.5 mm. The substrate has a thickness of 550 μm. It is composed of a single half-section of a channel and fin portion, with the adjacent surfaces set to symmetry boundary conditions. The top outer wall is heated by a constant heat flux, and the base wall is adiabatic. All other outer walls are also set to

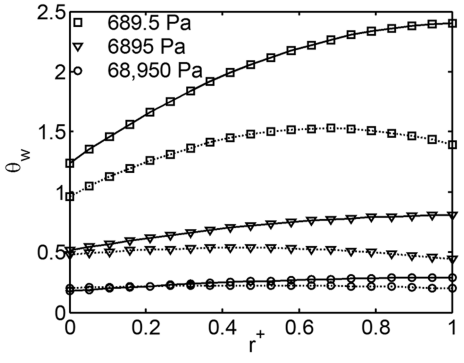

a) Nondimensional temperature

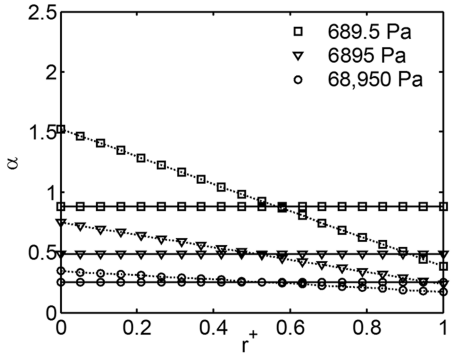

b) Aspect-ratio profile

Fig. 3 Minimizing peak temperature: linear profile of three-wall-heated constant temperature and fully developed flow for uniform channels (solid lines) and varying cross-sectional-area channels (dashed lines).

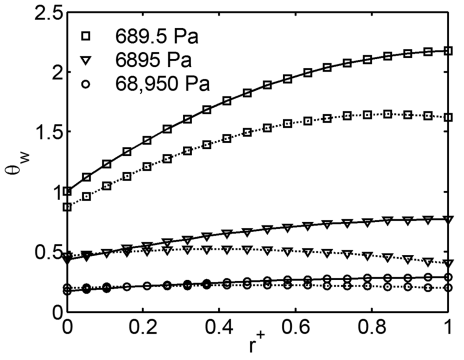

a) Nondimensional temperature

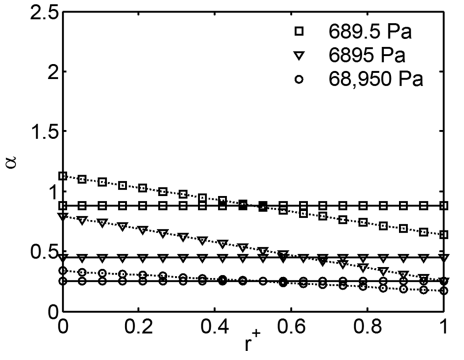

b) Aspect-ratio profile

Fig. 4 Minimizing peak temperature: linear profile of four-wall-heated constant temperature and fully developed flow for uniform channels (solid lines) and varying cross-sectional-area channels (dashed lines).

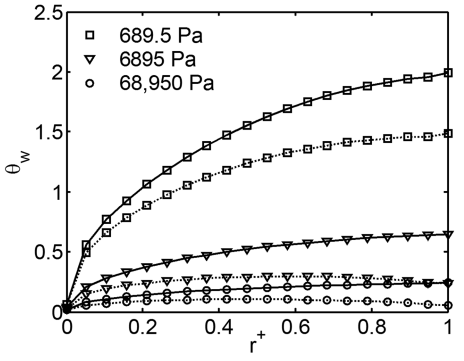

a) Nondimensional temperature

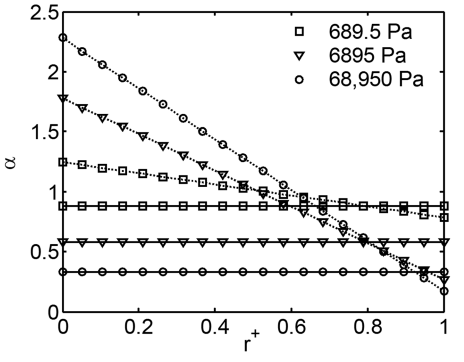

b) Aspect-ratio profile

Fig. 5 Minimizing peak temperature: linear profile of four-wall-heated constant temperature and thermally developing flow for uniform channels (solid lines) and varying cross-sectional-area channels (dashed lines).

Table 1 Benchmark grid study

Case	Mesh cells, $W_{chn} \times H_{chn} \times L_{chn}$	T_{out}, K	% change, $(T_{out,j+1} - T_{out,j})/T_{out,j}$
$j = 1$	$30 \times 40 \times 50$	308.9783	——
$j = 2$	$40 \times 100 \times 100$	309.1931	0.070
$j = 3$	$50 \times 160 \times 100$	309.225	0.010
$j = 4$	$50 \times 220 \times 120$	309.2292	0.001
$j = 5$	$60 \times 280 \times 150$	309.235	0.002

Table 2 Three-dimensional CFD simulation test matrix[a]

α_{in}	$H_{in} = 0.300$ ΔP_{fixed},[b] constant height, q_1'',[c] q_2'',[d] q_3''[e]	$\dot{m}_{fixed}$[f], constant flow rate, q_1''[c]	$W_{in} = 0.150$ ΔP_{fixed},[b] constant width, q_1''[c]	$\alpha_{in} = \alpha_{out} = 0.5$ ΔP_{fixed},[b] constant aspect ratio, q_1''[c]
0.4	$W_{in} = 0.120$	$W_{in} = 0.120$	$H_{in} = 0.375$	$W_{in} = 0.120$ and $H_{in} = 0.240$
0.45	$W_{in} = 0.135$	——	——	——
0.5	$W_{in} = 0.150$	$W_{in} = 0.150$	$H_{in} = 0.300$	$W_{in} = 0.150$ and $H_{in} = 0.300$
0.55	$W_{in} = 0.165$	——	——	——
0.6	$W_{in} = 0.180$	$W_{in} = 0.180$	——	$W_{in} = 0.180$ and $H_{in} = 0.360$
0.8	$W_{in} = 0.240$	$W_{in} = 0.240$	$H_{in} = 0.1875$	$W_{in} = 0.240$ and $H_{in} = 0.480$
1	$W_{in} = 0.300$	——	——	——

[a]Dimensions are in millimeters; $W_{out} = 0.15$ mm and $H_{out} = 0.30$ mm throughout. [b]$\Delta P_{fixed} = 6.9$ kPa [c]$q_1'' = 25$ W/cm^2 [d]$q_2'' = 43.75$ W/cm^2 [e]$q_3'' = 62.5$ W/cm^2 [f]$\dot{m}_{fixed} = 2.85$ kg/s

adiabatic. The inlet is set to pressure inlet or uniform velocity, depending on the case being evaluated, and the outlet is set to zero gauge pressure. The solid material is silicon ($k = 157$ W/m · K), and the fluid is water. The modeling assumptions are as follows: 1) steady-state flow and heat transfer, 2) laminar flow, 3) constant solid properties and temperature-dependent fluid properties, and 4) negligible radiation heat transfer.

The commercial package Gambit 2.0 is used for grid generation. A structured mesh with hexahedral elements is used in all of the test cases. The analysis is carried out using the commercial package FLUENT 6.1 to solve the continuity, momentum, and energy equations within the fluid and given by

$$\nabla \cdot (\rho \vec{V}) = 0 \tag{14}$$

$$\vec{V} \cdot \nabla(\rho \vec{V}) = -\nabla P + \nabla \cdot (\mu \nabla \vec{V}) \tag{15}$$

$$\vec{V} \cdot \nabla(\rho C_p T) = \nabla \cdot (k \nabla T) \tag{16}$$

and the conduction equation within the solid given by

$$\nabla \cdot (k \nabla T) = 0 \tag{17}$$

Discretization of pressure, velocity, and energy terms is through a second-order upwind scheme. Coupling of pressure and velocity is performed using the semi-implicit method for pressure-linked equations (SIMPLE) algorithm. Finally, the solution of the equations is through a segregated solver.

Benchmark Study and Grid Independency Evaluation

A benchmark investigation was performed to evaluate the efficacy of the modeling method and assumptions. The selected case was from the study by Lee and Garimella [20]. This study involved heat transfer investigations in a copper substrate with ten rectangular channels. The selected case consisted of 194-μm-wide by 884-μm-deep channels ($D_h = 318$ μm) that were 25.4 mm long. The simulated geometry and boundary conditions are similar to those intended for the radial heat sink. The geometry consisted of one-half of the channel width and wall thickness and the full channel length. Symmetry boundary conditions were applied on the side surfaces, a uniform heat flux was applied on the top surface, and adiabatic conditions were applied on the bottom surface. The flow was taken as laminar, with pressure boundary conditions and temperature-dependent fluid properties. The double-precision form of FLUENT was necessary to produce reasonably decreasing residuals. A number of grid densities were evaluated and through tracking the outlet temperature, a grid density of $50 \times 220 \times 120$ was deemed satisfactory. The results from the mesh evaluations are presented in Table 1. Based on this, the radial scheme was then evaluated with mesh densities of $50 \times 160 \times 100$ and $50 \times 220 \times 120$. The percent change in outlet temperature between the two mesh sizes was 0.001%, and so the $50 \times 220 \times 120$ grid size was selected for the study.

Three-Dimensional Conjugate Analysis Results

A number of configurations of varying cross-sectional-area channels were analyzed and compared with a uniform channel with an aspect ratio of 0.5. A summary of the test cases is listed in Table 2. For all of the test cases, the outlet aspect ratio is set to 0.5. The cases

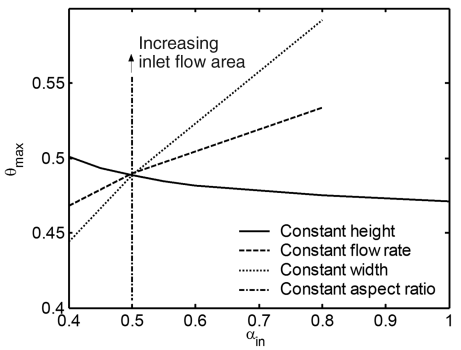

Fig. 6 Maximum surface temperature vs aspect ratio; $q'' = 25$ W/cm^2.

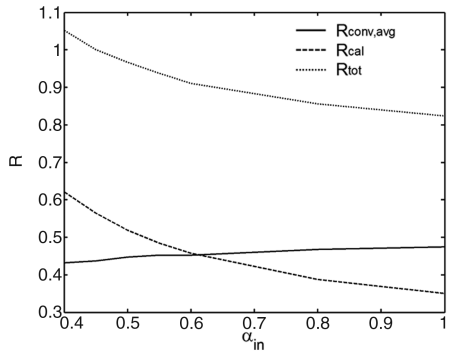

Fig. 7 Thermal resistance vs inlet aspect ratio for a constant-height case and $q'' = 25$ W/cm^2.

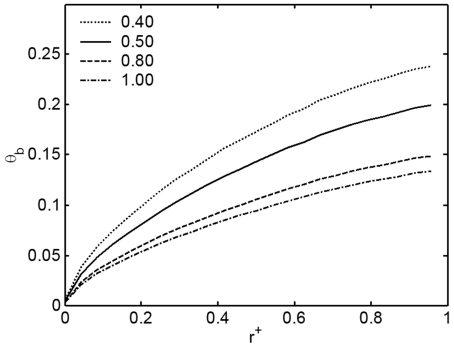

a) Constant channel height, various inlet aspect ratios

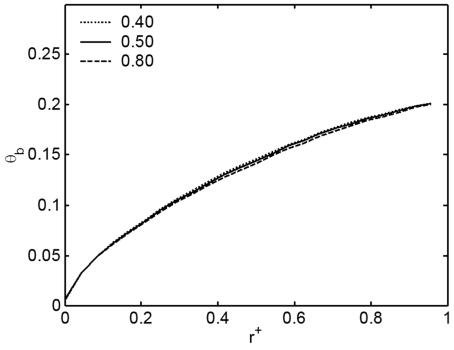

b) Constant mass flow rate, various inlet aspect ratios

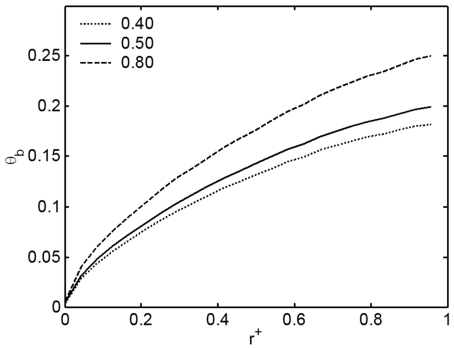

c) Constant channel width, various inlet aspect ratios

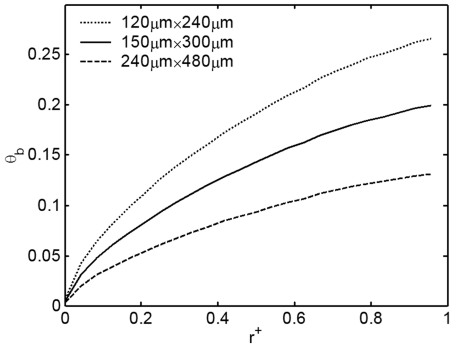

d) $\alpha = 0.5$, various inlet areas

Fig. 8 fluid bulk temperature; $q'' = 25$ W/cm^2.

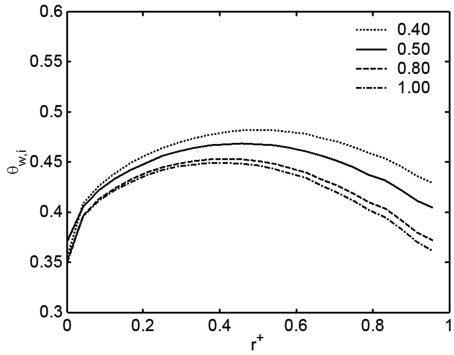

a) Constant channel height, various inlet aspect ratios

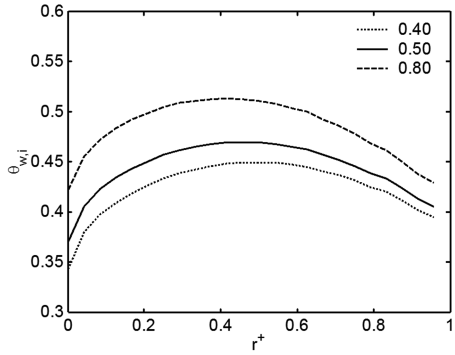

b) Constant mass flow rate, various inlet aspect ratios

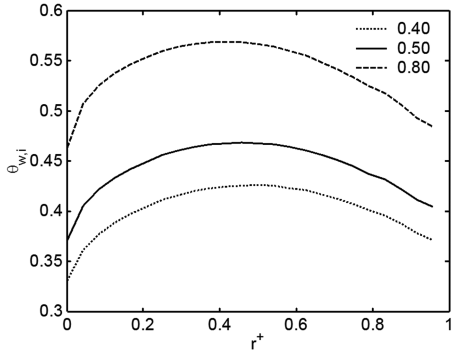

c) Constant channel width, various inlet aspect ratios

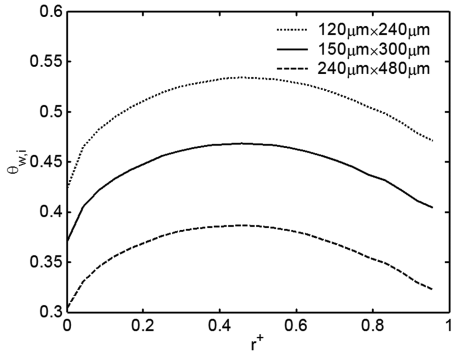

d) $\alpha_{in} = 0.5$, various inlet areas

Fig. 9 Three-wall-heated area average temperature; $q'' = 25$ W/cm^2.

considered are the influence of inlet width for aspect ratios ranging from 0.4 to 1.0, with a fixed pressure drop and a heat flux ranging from 25 to 62.5 W/cm^2. Also investigated is the influence of inlet width for inlet aspect ratios ranging from 0.4 to 1.0, but for a fixed mass flow rate and a heat flux of 25 W/cm^2. The influence of inlet height is investigated for inlet aspect ratios of 0.4, 0.5, and 1.0 for a fixed pressure drop and a heat flux of 25 W/cm^2. Finally, the last case considers a variable inlet height and width, with the inlet aspect ratio fixed at 0.5 for a fixed pressure drop and a heat flux of 25 W/cm^2.

Figure 6 presents the maximum surface temperature determined for the various test cases. For the fixed-height case, as the inlet width increases (and thus the inlet aspect ratio increases), a decreased peak temperature is obtained. Equivalently, for the fixed-width case, as the inlet height is increased (and thus the inlet aspect ratio increases), a decreased peak temperature is obtained. Also, for the case of a fixed

aspect ratio, increasing the inlet area decreases the peak temperature. Conversely, however, for the fixed-flow-rate case, increasing the inlet flow area increases the peak surface temperature. The average surface temperature plots showed trends similar to those of the maximum surface temperature.

In the fixed-pressure-drop cases, the decreasing peak temperature with increasing inlet flow area is primarily due to the increasing flow rate. Figure 7, as an example, shows the thermal resistance as a function of inlet aspect ratio for fixed-height channels with a fixed pressure drop. Increasing the inlet aspect ratio increases the mass flow rate, which in turn will decrease the calorimetric thermal resistance. Decreasing the inlet aspect ratio (diverging channels, $\alpha_{in} < 0.5$) will produce higher heat transfer coefficients and hence lower convective resistance. However, the benefit in heat transfer coefficient due to decreased channel-inlet size is not significant when compared with the mass flow benefit for increased channel-inlet size. This arises due to the restriction on the number of channels and is subsequently due to the restriction of the exit radius and the exit fin width. The mass flow alone, however, is not the only parameter determining the performance; the cross-sectional area and orientation are also determining factors. This is observed in the fixed-pressure-drop case of $\alpha_{in} = 0.6$ (0.3×0.18 mm) and $\alpha_{in} = 0.4$ (0.15×0.375 mm), which are fixed-height and fixed-width cases, respectively. Their inlet cross-sectional areas are within 4.2% of each other, with $\alpha_{in} = 0.6$ having the lower cross-sectional area. The mass flow rates, however, are reversed, with $\alpha_{in} = 0.4$ having a mass flow rate approximately 3.8% lower than $\alpha_{in} = 0.6$. Looking at Fig. 6, however, an aspect ratio of 0.4 produces a lower maximum temperature ($\theta_{max} = 0.44$) than with an aspect ratio of 0.6 ($\theta_{max} = 0.48$). This is primarily due to the differences in heat transfer coefficients, with the aspect ratio of 0.6 having an average Nusselt number of 8.6, whereas the aspect ratio of 0.4 produces an average Nusselt number of 14.0. Some benefit is also likely gained from a reduced upper-wall thickness for the 0.4 aspect-ratio case, due to a larger height.

In Figs. 8 and 9, the fluid bulk and inner-wall temperature characteristics of the radial heat exchanger are presented. The fluid bulk temperature is calculated based on an energy-weighted average, whereas the wall temperature is calculated based on an area-weighted average. In all cases, the fluid bulk temperature shows a nonlinear rise with increasing distance. A lower fluid bulk temperature rise is observed for cases with lower maximum wall temperatures. This is because the lower maximum temperature was obtained from an increase in mass flow. Because of a balance of energy for the same

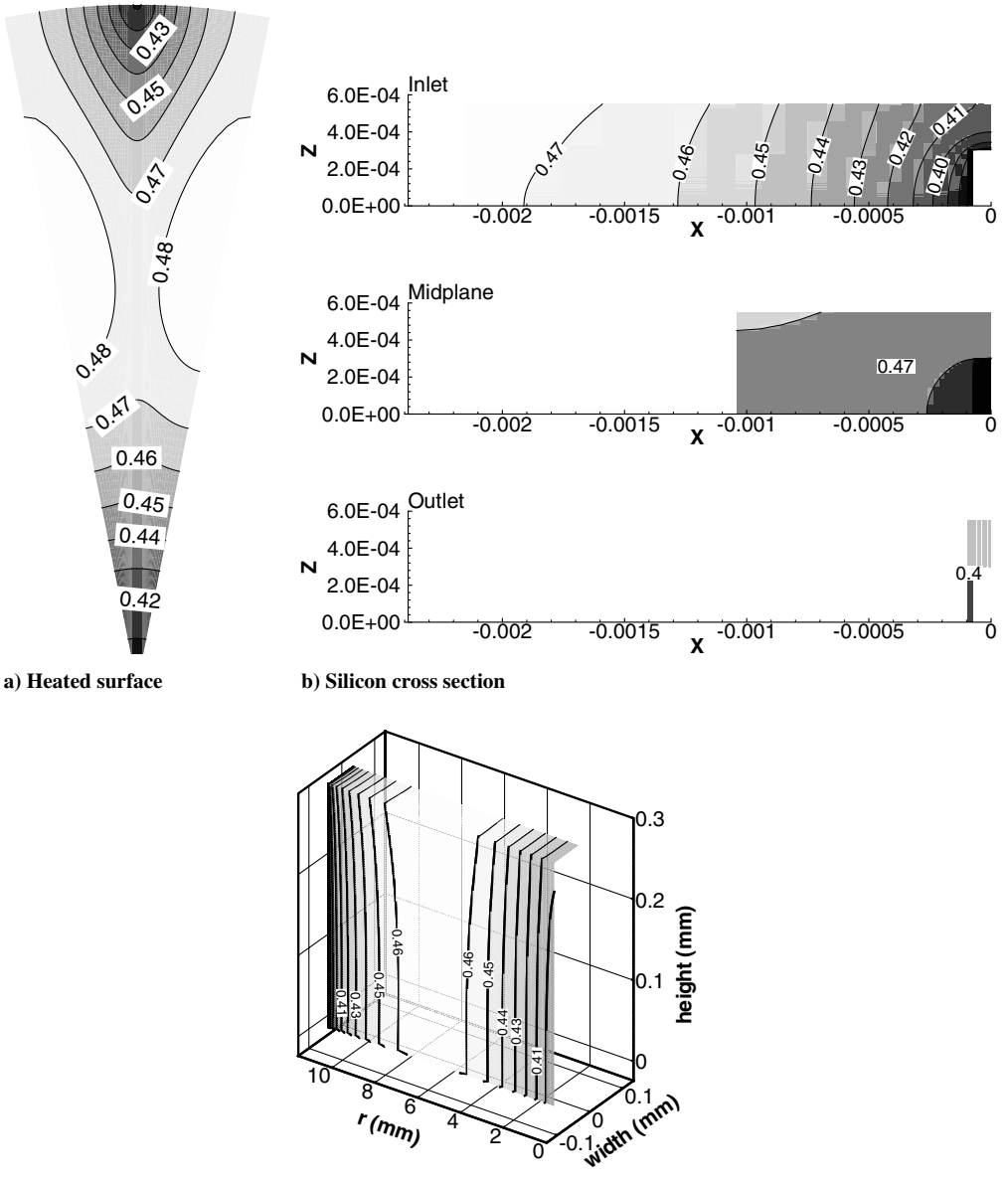

a) Heated surface

b) Silicon cross section

c) Inner wall

Fig. 10 Nondimensional temperature contours of a uniform channel' $\alpha = 0.5$ and $q'' = 25$ W/cm^2.

heat flux, a lower fluid bulk temperature rise will then be obtained when the mass flow rate is increased. This is also a consequence of the fluid property changes having minimal influence.

The inner wall shows a different temperature trend from the parallel-channel systems. The inner-wall temperature rises until approximately 50% of the length, then it drops. The rising wall temperature is expected, due to the increasing fluid temperature. The drop, however, arises from the thinning of the wall fins inherent in the radial configuration. In the case of a fixed mass flow rate (Figs. 8 and 9b), the fluid temperature rise is the same for all cases. However, a lower inner-wall temperature is obtained with an inlet aspect ratio of 0.4. This results from a higher Nusselt number for the 0.4 inlet-aspect-ratio channel, compared with the 0.8 inlet-aspect-ratio channel under the same mass flow conditions.

Contours of the temperature resulting in a uniform channel and a converging channel of the same aspect ratio ($\alpha = 0.5$) are presented in Figs. 10 and 11 respectively. Looking at the uniform channel case, Fig. 10a shows the surface temperature, with the channel located along the center. The surface temperature shows the elevated temperature to lie in the midstreamwise section, with the inlet and outlet temperatures both cooler. This is similarly related to the inner-wall temperature rise and drop discussed earlier (Fig. 9). Cross sections of the silicon wafer temperature gradients normal to both inner-wall surfaces are spread over a large distance at the inlet plane (Fig. 10b). For subsequent planes, the reduction in area causes both a lower temperature gradient and spread. The inner-wall temperature contours (Fig. 10 and 11c) show that the temperature is somewhat constant around the periphery in the inlet and outlet regions. However, as the center of the channel is approached, the periphery temperature is increasingly nonuniform. This is important to note when considering the use of analytical solutions such as those presented in Shah and London [19] for rapid channel optimization, because the majority of the solutions assume either a uniform temperature or uniform heat flux around the periphery. Comparing the uniform and converging channels, similar trends in the profiles are observed. The magnitudes, however, are significantly different, as expected from the averaged plots presented earlier.

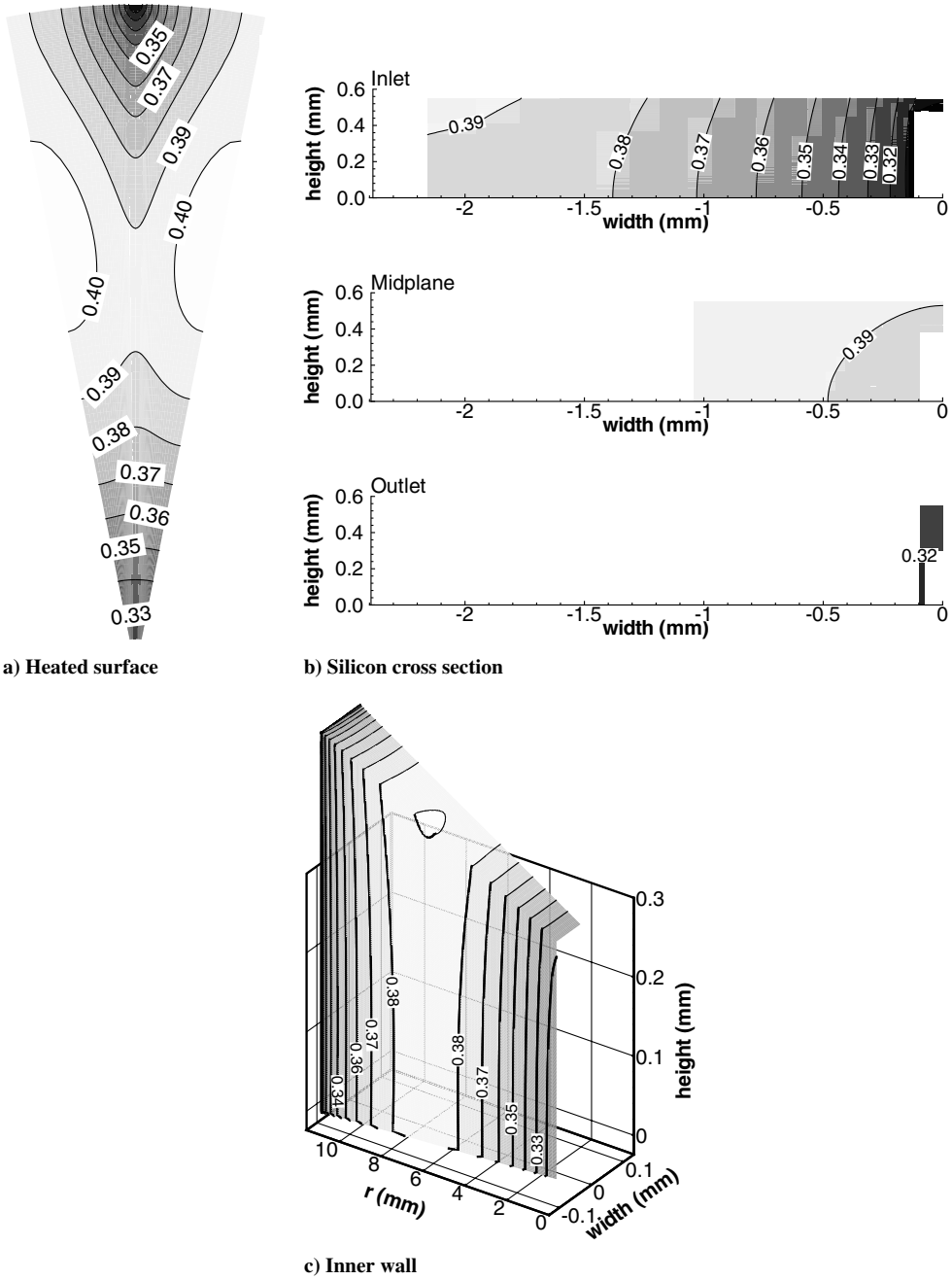

a) Heated surface

b) Silicon cross section

c) Inner wall

Fig. 11 Nondimensional temperature contours of a converging channel with an inlet area of 240 × 480 μm; $\alpha = 0.5$ and $q'' = 25$ W/cm^2.

The velocity contours for the symmetry plane of a uniform channel ($\alpha = 0.5$) under varying heat flux are presented in Fig. 12. With an increase in heat flux, higher velocities are attained. This is expected, because the fluid's viscosity decreases with increased temperature, providing a lower flow resistance. The velocity contours are also observed to be unsymmetrical with respect to the height, with higher velocity gradients obtained on the upper half of the channel. This is related once again to viscosity changes in the fluid, because the upper wall is heated and thus the fluid bulk temperature is hotter on the upper half. Similarly, Fig. 13 shows velocity contours for the symmetry plane for different geometrical configurations. Figure 13a is for a channel with decreasing width, Fig. 13b is for a channel with decreasing height, and in Fig. 13c, both the width and the height are decreasing. Increasing velocities are now obtained as a combination of a decreasing viscosity and a decreasing flow area. The case of simultaneously varying channel width and height has the highest velocity and, correspondingly, the highest mass flow rate and lowest maximum temperature.

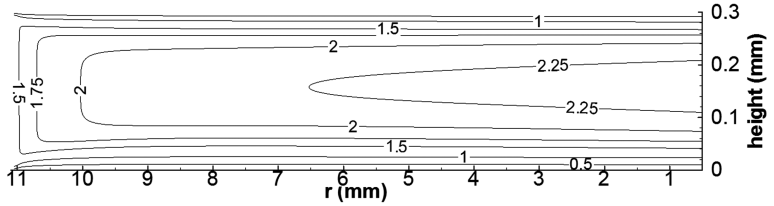

a) Q"=25.00 W/cm²

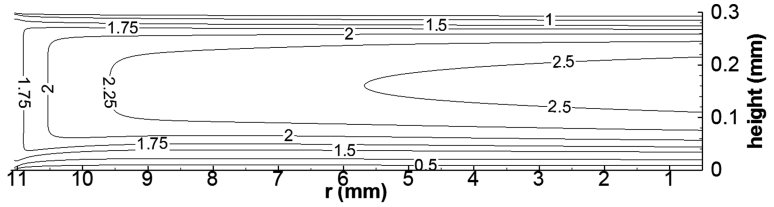

b) Q"=43.75 W/cm²

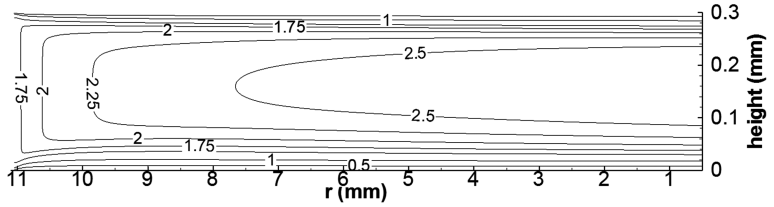

c) Q"=62.50 W/cm²

Fig. 12 Influence of heat flux on center-plane velocity (meters/second) for a uniform channel; $\alpha = 0.5$.

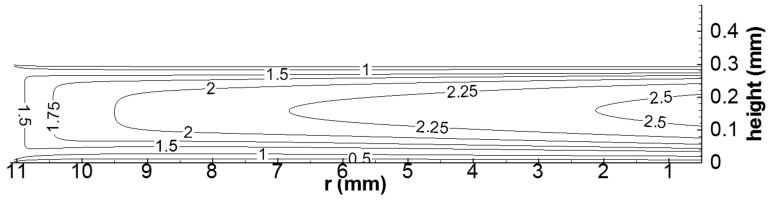

a) Varying channel width (fixed height), α_{in} = 0.6

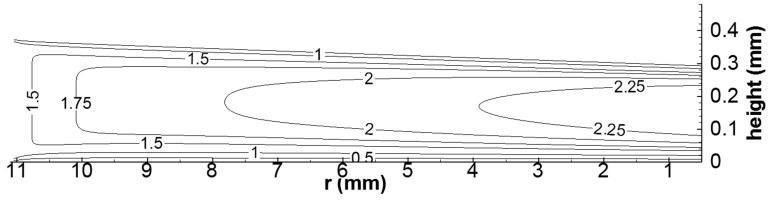

b) Varying channel height (fixed width), α_{in} = 0.4

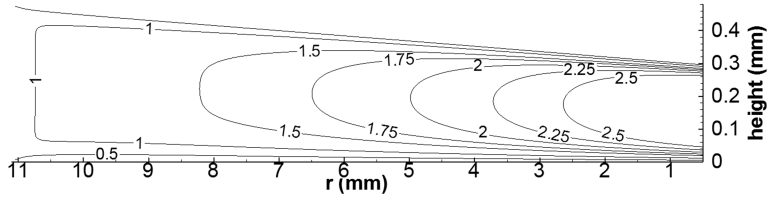

c) Varying channel width and height (fixed aspect ratio), $\alpha_{in} = \alpha_{out} = 0.5$

Fig. 13 Center-plane velocity (meters/second) for various geometrical configurations; $q'' = 25$ W/cm².

Thermal-Resistance Model Compared with Three-Dimensional Conjugate Analysis

The model developed by Bau [13] and the present adaptations for the thermal-resistance model, incorporating thermally developing flow and radially inward flow, have not been previously verified. These simplified models are advantageous for rapid geometry optimization; however, they contain a number of assumptions that may pose a limited applicability on their use. In this section, a comparison is made between these simplified models and a conjugate three-dimensional analysis, to explore the range of their applicability. The results for the conjugate three-dimensional analysis are derived from the previous section. In comparison with the thermal-resistance analysis, the three-dimensional model incorporates the fluid's temperature-dependent properties, solid and fluid axial conduction, and flow development.

Figure 14 compares the one-dimensional thermal-resistance model for parallel channels considering fully developed and thermally developing flows. The computational fluid dynamics (CFD) analysis is from the benchmark case, which consisted of uniform channels with hydraulic diameters of approximately 318 μm and aspect ratios of approximately 0.22. Good agreement is obtained between the CFD analysis and the thermally developing flow cases with respect to the general trend and the magnitude. The fully developed cases, however, largely overpredict the wall temperature. This overprediction is, in part, due to the higher heat transfer coefficients available in the flow development region, which subsequently lowers the wall temperature. The thermally developing cases, however, do not well predict the entrance or exit regions' wall temperatures. For the entrance, this is due to the thermal-resistance model not accounting for axial conduction, as is discussed later. For the exit, it is likely due to neglecting the fluid's viscosity decrease with distance. The decreasing viscosity will produce a higher local Reynolds number, which will increase the heat transfer coefficient while in the thermally developing regime.

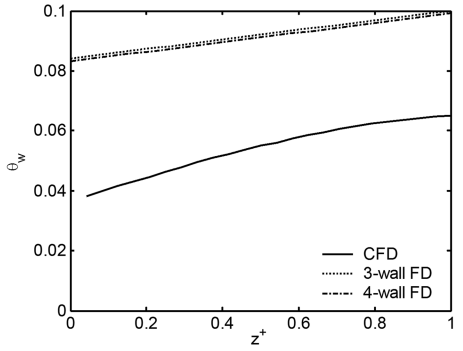

a) 3-wall and 4-wall heated fully developed (FD) flow models

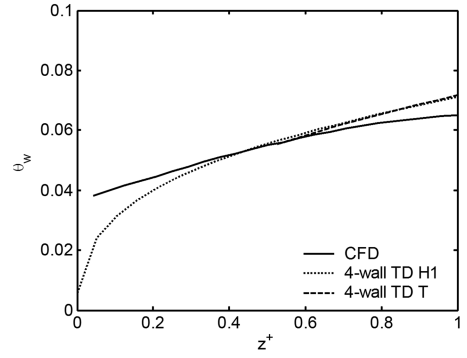

b) 4-wall heated thermally developing (TD) flow models; constant heat flux (H1) and constant temperature (T) boundary conditions

Fig. 14 Parallel uniform channel: one-dimensional thermal-resistance model compared with the three-dimensional conjugate analysis.

The thermally developing cases are for the four-wall-heated cases, whereas the CFD analysis is a three-wall-heated case. This difference, however, produces negligible differences, as is seen when comparing the three-wall-heated and four-wall-heated fully developed cases. Comparing the constant-heat-flux and constant-wall-temperature thermally developing cases, negligible differences are observed. However, the constant-heat-flux case, which was used in the previous sections, is advantageous because it is available in a wider range of nondimensional streamwise coordinates ($z^* = z/(RePrD_h)$, to better reproduce the inlet characteristics for a wide range of aspect ratios. These results demonstrated that for parallel-channel systems, when optimizing for a channel with uniform cross section, consideration of the thermal entrance region is imperative for accurate comparisons. This conclusion is also expected for parallel channels with varying cross-sectional areas.

Figure 15 compares the fully developed and thermally developing one-dimensional thermal-resistance models with the three-dimensional conjugate analysis for radially-inward-flow configurations. Two cases are considered: a uniform channel ($\alpha = 0.5$) and a converging channel with a unity inlet aspect ratio. Similar to the parallel-channel case, the trend and magnitude is not well predicted by the fully developed flow cases, when compared with the three-dimensional conjugate analysis. In addition, however, the thermally developing cases do not provide a good match with this analysis. To investigate this further, plots of the resulting heat flux in the conjugate analysis compared with the expected one-dimensional uniform heat flux are presented in Fig. 16. It is observed in this figure that in both the parallel and radial channel cases, the heat flux is nonuniform. However, in the case of the radial channel, it is significantly greater. The mean deviation, defined as

$$\mathrm{MD} = \frac{1}{L_{\mathrm{chn}}} \int_0^{L_{\mathrm{chn}}} (q''_{\mathrm{CFD}} - q''_{\mathrm{1\text{-}D,uniform}})\, \mathrm{d}z \tag{18}$$

is calculated to be 25% for the radial channel, compared with 2.9% for the parallel channel. This nonuniformity is due primarily to axial heat conduction within the solid traveling toward the channel entry. This can be expected (particularly, in the case of the radial channels),

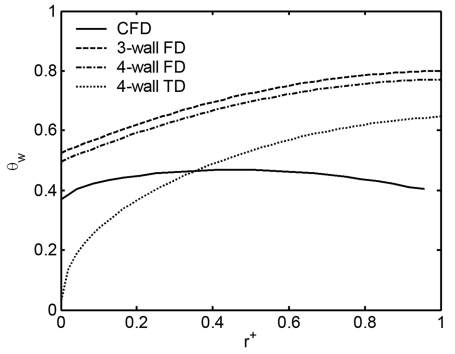

a) Uniform channel, $\alpha_{in} = 0.5$

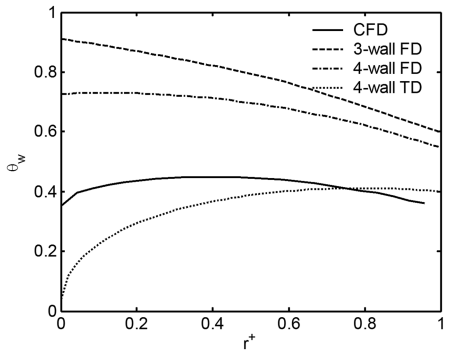

b) Converging channel, $\alpha_{in} = 1.0$

Fig. 15 Radial channel: one-dimensional thermal-resistance model compared with the three-dimensional conjugate analysis.

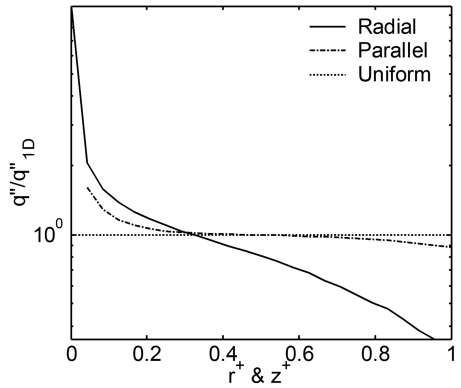

Fig. 16 Resulting inner-wall heat flux distribution from three-dimensional conjugate analysis compared with uniform one-dimensional heat flux distribution.

because a large part of the volume is solid and this region gets larger toward the inlet. In summary, the one-dimensional radial model, which is an adaptation of the one-dimensional parallel-channel model, does not provide good predictability of the surface temperature, due to the assumption of negligible wall thickness. This negligible wall thickness translates into an assumption of uniform heat flux at the inner-wall surface, which is a stark difference from the physical reality.

Comparison of Thermal Performance

In this section, the thermal performance of the radial microchannel heat exchanger with varying cross-sectional-area channels is compared with other radial and parallel-channel heat sinks/exchangers. The chosen measurand is the maximum thermal resistance vs the required pumping power. The thermal resistance is defined as

$$R_{\max} = \frac{T_{w,\max} - T_{\text{in}}}{Q} \tag{19}$$

where the pumping power is the product of the flow rate and pressure drop. Figure 17 compares the present results with data from other experimental and numerical investigations. The open symbols are from experimental measurements with parallel-channel schemes, the cross and plus symbols are from numerical investigations with radially-outward-flowing schemes, and the closed symbols are the present numerical investigations of fixed aspect ratio and fixed width for a constant pressure drop. For low pumping power, the present scheme shows better performance than the parallel-channel scheme of Paris et al. [21]. Additionally extrapolating the radial schemes by Wang et al. [6] to lower pumping, the present scheme also shows better performance. Extrapolating the results of Harms et al. [22] to a lower pumping power, the performance of this parallel-channel scheme tends to be similar to the presently proposed radial scheme. Overall, the present radial scheme has a performance that is

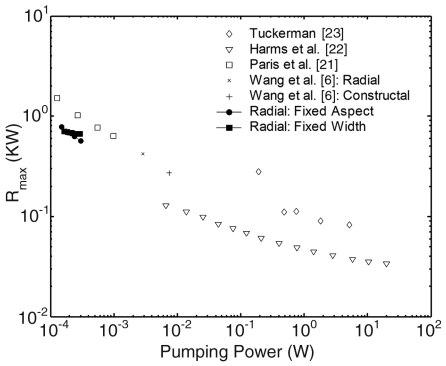

Fig. 17 Comparison of thermal performance for various geometrical configurations; $q'' = 25\ \text{W/cm}^2$.

equivalent to or better than other radial and parallel-channel-pumped cooling schemes at low pumping power. These findings, however, are based on a comparison with a limited data pool, because few studies (particularly, of radial configurations) are available.

Conclusions

The performance of a radially inflowing microchannel-heat-exchanger scheme was investigated numerically. Unique to this scheme was the consideration of channels with axially varying cross sections.

A one-dimensional thermal-resistance model was explored for rapid optimization of channels with varying cross sections for radially inflowing microchannel heat exchangers. This model is an adaptation of a previous model for parallel-channel systems. In general, the analysis shows that linearly converging channels are superior to uniform channels. However, the model predictions do not fare well when compared with the three-dimensional conjugate analysis. This is mainly due to the assumption of negligible wall-thickness thermal resistance, which neglects the significant axial conduction possible in a radially inflowing configuration. Future studies should develop a thermal-resistance model accounting for axial conduction, to aid in the rapid optimization of channels with varying cross sections in radial configurations.

Three-dimensional conjugate analysis shows that when constrained by a fixed channel-outlet area, increasing the channel-inlet area will improve the thermal performance. This is due to increased mass flow providing for a decreased calorimetric resistance. The use of this scheme is found to be advantageous in scenarios of low-pumping-power requirements. Future works are recommended to explore this scheme further, both numerically and experimentally.

References

[1] Li, S., Fozdar, D., Ali, M. F., Li, H., Shao, D., Vykoukal, D. M., Vykoukal, J., Floriano, P. N., Olsen, M., McDevitt, J. T., Gascoyne, P. R. C., and Chen, S., "A Continuous-Flow Polymerase Chain Reaction Microchip with Regional Velocity Control," *Journal of Microelectromechanical Systems*, Vol. 15, No. 1, 2006, pp. 223–236. doi:10.1109/JMEMS.2005.859083

[2] Epstein A. H., "Millimeter-Scale, MEMS Gas Turbine Engines," *Proceedings of the ASME Turbo Expo 2003*, Vol. 4, American Society of Mechanical Engineers, New York, 2003, pp. 669–696.

[3] Tuckerman, D. B., and Pease, R. F. W., "High-Performance Heat Sinking for VLSI," *IEEE Electron Device Letters*, Vol. 2, No. 5, 1981, pp. 126–129. doi:10.1109/EDL.1981.25367

[4] Kosar, A., and Peles, Y., "Thermal-Hydraulic Performance of MEMS-Based Pin Fin Heat Sink," *Journal of Heat Transfer*, Vol. 128, No. 2, 2006, pp. 121–131. doi:10.1115/1.2137760

[5] Peles, Y., Kosar, A., Mishra, C., Kuo, C., and Schneider, B., "Forced Convective Heat Transfer Across a Pin Fin Micro Heat Sink," *International Journal of Heat and Mass Transfer*, Vol. 48, No. 17, 2005, pp. 3615–3627. doi:10.1016/j.ijheatmasstransfer.2005.03.017

[6] Wang, X., Yap, C., and Mujumdar, A., "Laminar Heat Transfer in Constructal Microchannel Networks with Loops," *Journal of Electronic Packaging*, Vol. 128, No. 3, 2006, pp. 273–280. doi:10.1115/1.2229228

[7] Chen, Y., and Cheng, P., "An Experimental Investigation on the Thermal Efficiency of Fractal Tree-Like Microchannel Nets," *International Communications in Heat and Mass Transfer*, Vol. 32, No. 7, 2005, pp. 931–938. doi:10.1016/j.icheatmasstransfer.2005.02.001

[8] Alharbi, A., Pence., and Cullion, R., "Thermal Characteristics of Microscale Fractal-Like Branching Channels," *Journal of Heat Transfer*, Vol. 126, No. 5, 2004, pp. 744–752. doi:10.1115/1.1795236

[9] Pence, D. V., "Reduced Pumping Power and Wall Temperature in Microchannel Heat Sinks with Fractal-Like Branching Channel Networks," *Microscale Thermophysical Engineering*, Vol. 6, No. 4, 2002, pp. 319–330. doi:10.1080/10893950290098359

[10] Xu, J. L., Gan, Y. H., Zhang, D. C., and Li, X. H., "Microscale Heat Transfer Enhancement Using Thermal Boundary Layer Redeveloping Concept," *International Journal of Heat and Mass Transfer*, Vol. 48, No. 9, 2005, pp. 1662–1674. doi:10.1016/j.ijheatmasstransfer.2004.12.008

[11] Cho, E. S., Koo, J., Jiang, L., Prasher, R. S., Kim, M. S., Santiago, J. G., Kenny, T. W., and Goodson, K. E., "Experimental Study on Two-Phase Heat Transfer in Microchannel Heat Sinks with Hotspots," *Nineteenth Annual IEEE Semiconductor Thermal Measurement and Management Symposium*, Inst. of Electrical and Electronics Engineers, Piscataway, NJ, 2003, pp. 242–246.

[12] Jiang, L., Koo, J. M., Wang, E., Bari, A., Cho, E. S., Ong, W., Prasher, R. S., Maveety, J., Kim, M. S., Kenny, T. W., Santiago, J. G., and Goodson, K. E., "Cross-Linked Microchannels for VLSI Hotspot Cooling," *ASME International Mechanical Engineering Congress and Exposition*, American Society of Mechanical Engineers, New York, 2002, pp. 13–17.

[13] Bau, H. H., "Optimization of Conduits' Shape in Micro Heat Exchangers," *International Journal of Heat and Mass Transfer*, Vol. 41, No. 18, 1998, pp. 2717–2723. doi:10.1016/S0017-9310(98)00003-9

[14] Mantion, M. J., "Low Reynolds Number Flow in Slowly Varying Axisymmetric Tubes," *Journal of Fluid Mechanics*, Vol. 49, No. 3, 1971, pp. 451–459. doi:10.1017/S0022112071002192

[15] Lauga, E., Stroock, A. D., and Stone, H. A., "Three-Dimensional Flows in Slowly Varying Planar Geometries," *Physics of Fluids*, Vol. 16, No. 8, 2004, pp. 3051–3062. doi:10.1063/1.1760105

[16] Brod H., "Invariance Relations for Laminar Forced Convection in Ducts with Slowly Varying Cross Section," *International Journal of Heat and Mass Transfer*, Vol. 44, No. 5, 2001, pp. 977–987. doi:10.1016/S0017-9310(00)00156-3

[17] Ekkad, S. V., Pamula, G., and Shantiniketanam, M., "Detailed Heat Transfer Measurements Inside Straight and Tapered Two-Pass Channels with Rib Turbulators," *Experimental Thermal and Fluid Science*, Vol. 22, No. 3, 2000, pp. 155–163. doi:10.1016/S0894-1777(00)00022-4

[18] Muwanga, R. S., "Experimental Study on Heat Transfer Characteristics of Microchannel Systems Using Liquid Crystal Thermography," Ph.D. Dissertation, Concordia Univ., Montreal, 2007.

[19] Shah, R. K., and London, A. L., "Laminar Flow Forced Convection in Ducts," *Advances in Heat Transfer*, Academic Press, New York, 1978.

[20] Lee, P., and Garimella, S. V., "Thermally Developing Flow and Heat Transfer in Rectangular Microchannels of Different Aspect Ratios," *International Journal of Heat and Mass Transfer*, Vol. 49, Nos. 17–18, 2006, pp. 3060–3067. doi:10.1016/j.ijheatmasstransfer.2006.02.011

[21] Paris, A. D., Birur, G. C., and Green, A. A., "Development of MEMS Microchannel Heat Sinks for Micro/Nano Spacecraft Thermal Control," *Proceedings of the International Mechanical Engineering Congress and Exposition (IMECE 2002)*, Vol. 4, American Society of Mechanical Engineers, New York, 2002, p. 8.

[22] Harms, T. M., Kazmierczak, M. J., and Gerner, F. M., "Developing Convective Heat Transfer in Deep Rectangular Microchannels," *International Journal of Heat and Fluid Flow*, Vol. 20, No. 2, 1999, pp. 149–157. doi:10.1016/S0142-727X(98)10055-3

[23] Tuckerman, D. B., "Heat Transfer Microstructures for Integrated Circuits," Ph.D. Thesis, Stanford Univ., Stanford, CA, 1984.